RSC Advances

PAPER

View Article Online
View Journal | View Issue

Cite this: *RSC Adv.*, 2015, **5**, 4135

Facial synthesis of hexagonal metal oxide nanoparticles for low temperature ammonia gas sensing applications

Ishpal Rawal*

Received 20th October 2014
Accepted 8th December 2014

DOI: 10.1039/c4ra12747a

www.rsc.org/advances

A surfactant assisted facial hydrothermal process has been employed for the synthesis of rutile and wurtzite phase SnO_2 and ZnO nanoparticles, respectively, confirmed by X-ray diffraction studies. High resolution transmission electron microscopy studies revealed the formation of ~15 and 20 nm of SnO_2 and ZnO nanoparticles, respectively, whereas, the structural analysis was done *via* Fourier transform infrared (FTIR) and Raman spectroscopy studies that suggested the minor doping of surfactant and surface adsorption of environmental oxygen. The gas sensing response of the prepared nanoparticles has been measured in ammonia environment and the sensing responses of the SnO_2 and ZnO nanoparticles are found to be 4.53 and 3.96%, respectively, at 46 ppm of ammonia. The mechanism of interaction of ammonia with metal oxide nanoparticles has been investigated through FTIR and Raman spectroscopic measurements performed in ammonia environment.

1. Introduction

Zinc oxide (ZnO) and tin oxide (SnO_2) are wide band gap multifunctional semiconductor materials widely used in opto-electronic devices, solar cells, gas sensors, and batteries, *etc.*[1–14] Metal oxides are well known for their excellent gas sensing ability to detect a variety of gases/chemical vapors with long term durability and exception selectivity.[4,7,8,11–14] The real interest in metal oxide sensors was started back in 1962 and since then, numerous semiconducting metal oxides are investigated for gas sensing application in different shapes, sizes and forms to satisfy the demand of high sensitivity, fast response with improved surface to volume ratio, low cost, low power consumption, relatively lower operating temperature with the possibility of miniaturization and high compatibility with the microelectronic processing. Nanostructural forms of such metal oxide materials are of considerable interest due to their shape, size and structure dependent properties having improved surface to volume ratio.[14,17] *e.g.* Zhang and Liu[14] reported the size dependent gas sensing properties of SnO_2 particles, whereas, Jiang *et al.*[17] were used their controlled sized mono-dispersed SnO_2 nanoparticles for electrocatalytic application. Out of numerous reports on gas sensitivity of metal oxides, more than half of the reports are based on SnO_2 and ZnO for the detection of different gases such as NO_x, NH_3, ethanol, methanol, acetone, chloroform, CO, H_2S, *etc.* due to their excellent gas sensing ability.[4,7,8,11–22] But these materials are still straggling with the problem of high operating temperature (150–450 °C), which require special attention. *e.g.* Shouli *et al.*[16] investigated the gas sensing behavior of ZnO nanorods in the temperature range of 150–450 °C towards different chemical vapors such as ethanol, acetone, toluene, benzene, and NO_2, *etc.* and observed that the prepared nanorods have highest sensing response at ~400 °C towards NO_2. Bagal *et al.*[7] investigated the sensing behavior of Pd doped SnO_2 nanoparticles in different chemical environments such as ammonia, ethanol, acetone and LPG in the temperature range of 200–450 °C and observed highest sensing response at 250 °C. Besides this, several other researchers used different metal oxides (Al_2O_3, ZrO_2/Eu^{3+}, Y_2O_3, ZrO_2, Cr_2O_3 ZnO and MgO, *etc.*) and their nanocomposites in different compositions for optical (cataluminescence and chemiluminescence, *etc.*) sensors to detect various types of chemical vapors.[10,18–22] These chemical vapors not only responsible for environmental pollution which causes acid rain or greenhouse type of effects but their direct exposure creates serious health problems. Ammonia is one of the most toxic gases having a threshold limit of 25 ppm, whose short term exposure can damage the human respiratory system, eyes and skin, whereas, long term can cause to death. Ammonia is widely used in different chemical industries, petrochemical industries and various other manufacturing units of plastics, explosives, textiles, pesticides, dyes, *etc.* Thus, a low level detection of it, in working environment is essential.[23] Khun *et al.*[11] reported the excellent ammonia gas sensing properties of SnO_2 thick film, whereas, Rout *et al.*[12] demonstrated the ammonia gas sensing properties of different nanostructures of metal oxides (ZnO, SnO_2, In_2O_3) at different temperatures 100–300 °C and found a maximum response at 300 °C. Thus, the high operating temperature of these metal oxides always inspired materials

Department of Physics, Kirori Mal College, University of Delhi, Delhi-110007, India. E-mail: rawalishpal@gmail.com

researchers towards searching of materials of structural diversity and controlled dimensionality for low temperature gas sensors. The synthesis of such materials of structural diversity and controlled dimensionality includes several synthetic routes such hydrothermal,[11,12] surfactant directed,[24–26] template assisted,[27] *etc.*, and can be modified according to the requirement. Conventional methods generally face some agglomeration problem with nanostructures, which can be resolved out by using some capping agents (surfactants) or templates. These capping agents/templates are not only helped to avoid agglomeration, but also decide the shape and dimensionality of the prepared nanostructures and thus, are of great interest in nanostructure formation.[24–27] Thus, these materials always are remained the center of attention for materials scientist and field is still opened to welcome new methodology. Despite of enough available literature on such metal oxides for optical, electrical and gas sensing applications,[1–14] spectroscopy based gas sensing mechanism is not fully established. Recently, we have used Raman spectroscopy technique to understand gas sensing mechanism in polymeric materials in ammonia environment,[28] but such studies are rare in metal oxides.

In view of this, in the present investigation, we have prepared ZnO and SnO_2 based metal oxide nanoparticles and investigated their gas sensing behavior *via* electrical and vibrational spectroscopic (Fourier transform infrared (FTIR) and Raman) techniques in ammonia environment. Moreover, their structural and morphological studies are also performed to confirm the formation of nanostructural form with controlled structurality and dimensionality.

2. Experimental section

Synthesis of metal oxide nanoparticles

A facial hydrothermal process was used for the synthesis of SnO_2 and ZnO nanoparticles. In a typical synthesis process of ZnO nanoparticles, 50 mM salt solution of zinc acetate was prepared in 100 ml methanol and refluxed for 2 h at 150 °C. Thereafter, 30 mM solution of Olay amine was added to it followed by the addition of 1 M NH_3, which provided hydroxide anions and helps to increase the pH value of the solution.[16,29,30] A separately prepared solution of reducing agent KOH (50 mM) was added to it drop-wise and the reaction was carried out for 2 h at same temperature. After that, solution was cooled down to room temperature naturally and centrifuged at 7000 rpm to separate out the prepared ZnO nanoparticles, washed several times with distilled water and dried at 80 °C for 12 h. Finally, the prepared nanoparticles were annealed at 300 °C for 4 h. The typical synthesis of ZnO nanocrystal in aqueous solution following the reaction mechanism of types[30]

$$NH_3 + H_2O \rightarrow NH_4^+ + OH^- \quad (1)$$

$$Zn^{2+} + 4OH^- \rightarrow Zn(OH)_4^{2-} \quad (2)$$

$$Zn^{2+} + 4NH_3 \rightarrow Zn(NH_3)_4^{2+} \quad (3)$$

$$Zn(OH)_4^{2-} \rightarrow ZnO + H_2O + 2OH^- \quad (4)$$

$$Zn(NH_3)_4^{2+} + 2OH^- \rightarrow ZnO + 4NH_3 + H_2O \quad (5)$$

The synthesis of SnO_2 nanoparticles has also been made by the above discussed method differing only by using of $SnCl_4 \cdot 5H_2O$ *in lieu* of zinc acetate and thus, the chemical reactions mentioned above can also be extended for the synthesis of SnO_2 nanocrystals as.

$$Sn^{4+} + 4OH^- \rightarrow Sn(OH)_4 \quad (6)$$

$$Sn(OH)_4 \rightarrow SnO_2 + 2H_2O \quad (7)$$

Characterization of prepared nanoparticles

X-ray diffraction studies have been performed on the prepared nanoparticles at D8 discover (ASX-Bruker), X-ray diffractometer using Cu-Kα radiation. The molecular structural analysis of the prepared nanoparticles was carried out by Fourier transform infrared (FTIR) spectroscopy recorded at Perkin-Elmer-RX1 spectrum and Raman spectroscopy carried out at Renishaw In-Via Reflex micro Raman spectrometer. The particle size analysis was made *via* high resolution transmission electron microscopy (HRTEM) study carried out at FEI, Tecnai G2 F30-STWIN. The low temperature (60–200 °C) interaction of metal oxide (SnO_2 and ZnO) nanoparticles with ammonia gas was investigated through electrical measurements performed in ammonia environment, whereas, for the investigation of gas sensing mechanism with metal oxide nanoparticles, spectroscopic (FTIR and Raman) measurements were carried out at room temperature in ammonia environment.

3. Results and discussion

Structural analysis

The structural analysis of the prepared metal oxide (SnO_2 and ZnO) nanoparticles was carried out using XRD measurements. Fig. 1 shows the XRD patterns of the prepared SnO_2 and ZnO nanoparticles. The XRD pattern of SnO_2 nanoparticles predominantly comprises of five broad peaks located at ~26, 31, 39, 51 and 68° associated with the (*hkl*) planes (110), (101), (200),

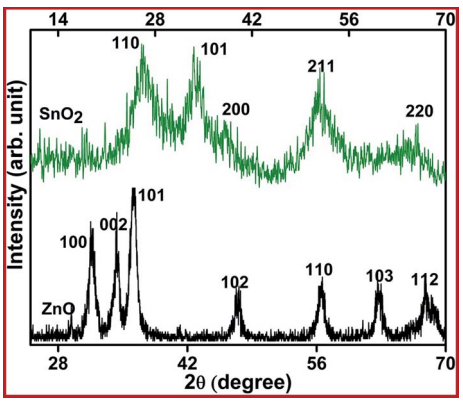

Fig. 1 XRD patterns of SnO_2 and ZnO nanoparticles.

(211) and (220), respectively. The observed peaks are indicative of the formation of rutile phase (JCPDS 41-1145) SnO_2.[7,11,12] On the other hand, XRD pattern of ZnO nanoparticles consists of several broad peaks located at ~31.5, 34.34, 36, 47.4, 56.54, 62.68 and 67.76° and are attributed to the (*hkl*) planes (100), (002), (101), (102), (110), (103) and (112), respectively. The observed peaks are well matched with wurtzite phase (JCPDS data card no. 36-1451) of ZnO.[10,12,13,31] The XRD peaks for both the samples have sufficient broadening that indicating the formation of metal oxide nanoparticles and the crystallites size for both the samples was calculated *via* standard Scherrer formula. The average crystallite sizes for SnO_2 and ZnO are ~12 and 15 nm, respectively.

Fig. 2(a) and (b) show the SEM micrographs of the SnO_2 and ZnO nanoparticles, respectively. The large agglomerations of the small sized (<50 nm) nanoparticles has been observed from both the micrographs. Due to small size of the nanoparticles, it becomes difficult to define the shape of the nanoparticles. Therefore, to explore the shape and size of the nanoparticles, HRTEM studies have been performed on both the samples (shown in Fig. 3(a)–(d)). In both cases of metal oxides (SnO_2 and ZnO) hexagonal shaped nanoparticles are observed that might be due to follow of similar synthetic route and formation of similar surfactant cages for capping the nanoparticles *i.e.* the prepared samples hold a 6-fold symmetry. The particle sizes for SnO_2 and ZnO nanoparticles are about 15 and 20 nm, respectively, evaluated by HRTEM studies (Fig. 3(a)–(d)). The average particle sizes evaluated through HRTEM studies are very close to the crystallite sizes (~12 nm for SnO_2 and ~15 nm for ZnO) calculated by using Scherrer's formula from XRD studies. The selected area electron diffraction (SAED) patterns of both the SnO_2 and ZnO samples comprise of well defined rings (inset of respective Fig. 3(b) and (d)), which further confirms the high crystalline nature of the prepared samples. The well visualized lattice planes (Fig. 3(b) and (d)) in the nanocrystallites, further support the crystalline nature of the synthesized samples. However, some diffused amorphous structures are also present around the nanocrystals in both samples that might be due to traces of surfactant used for the capping of these nanoparticles. The interplanar spacing for SnO_2 nanocrystal (inset of Fig. 3(a)) is about 0.26 nm which corresponds to (101) plane of the rutile SnO_2,[7,24,27] whereas, the interplanar spacing for ZnO nanocrystal is about 0.518 nm which corresponds to (0001) plane of wurtzite ZnO.[30,32,33] In high pH solution, Zn^{2+} are readily react with OH^- anions to form a stable $Zn(OH)_4^{2-}$ complexes (reaction (2)) or with NH_3 to form $Zn(NH_3)_4^{2+}$ ions (reaction (3)) and finally

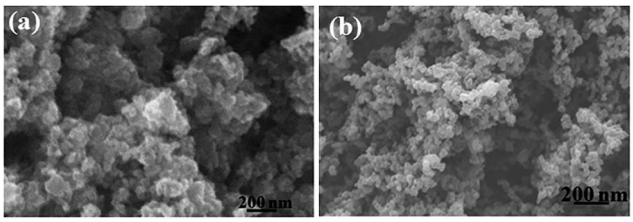

Fig. 2 SEM micrographs of (a) SnO_2 (b) ZnO nanoparticles.

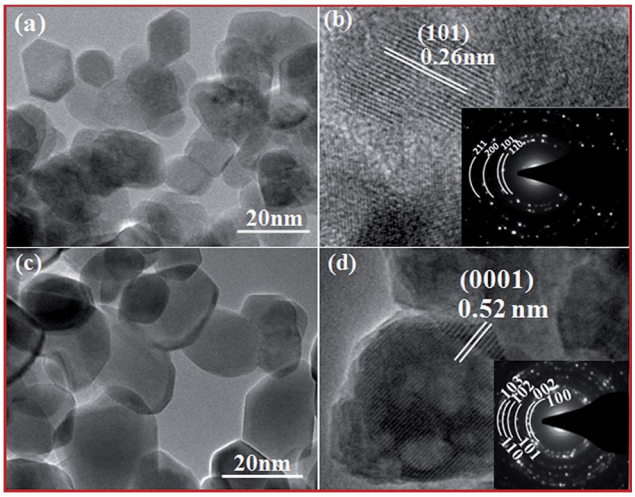

Fig. 3 TEM images of (a) SnO_2, (b) HRTEM micrograph SnO_2 (inset: SEAD pattern of SnO_2), TEM images of (c) ZnO and (d) HRTEM micrograph of ZnO (inset SEAD pattern of ZnO) nanoparticles.

produces ZnO crystals.[30] The synthesized ZnO crystal structure have hexagonally close packed zinc and oxygen atoms.[30] Xu *et al.*[32] used various capping agents for the growth of different shape and size ZnO nanostructures by considering the fact that the capping agents can blocks certain faces and promote the growth of other faces. They have also well explained the mechanism of anisotropic growth of ZnO crystals along (0001) direction. The wurtzite structure of ZnO crystal has number of alternating planes of 4-fold coordinated O^{2-} and Zn^{2+} ions, stacked alternatively along the *c* axis. The typical ZnO crystal generally consists of a top tetrahedron corner exposed polar Zn plane (0001), a basal polar oxygen plane (0001) and a non-polar six symmetric (1010) face/plane parallel to *c*-axis or (0001) direction.[16,30,32] These faces have different polarities and the non-polar (1010) faces, which are thermodynamically quite stable as compared to polar (0001) faces having surface dipoles. Due to high electrostatic force of attraction, the negative ions in the solution are adsorbed on the positive polar face of (0001) plane, which results in anisotropic growth of ZnO crystal along the (0001) direction.[16,30,32]

The molecular structure of the prepared nanoparticles has been investigated through FTIR and Raman spectroscopy (shown in Fig. 4) techniques. FTIR spectrum of SnO_2 nanoparticles (Fig. 3(a)) consists of an intense broad band around

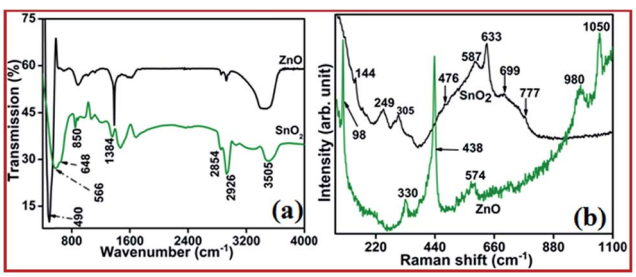

Fig. 4 (a) FTIR and (b) Raman spectra of SnO_2 and ZnO nanoparticles.

566 cm^{-1} with mark shoulder at 648 cm^{-1} that are attributed to Sn–O–Sn stretching vibration and O–Sn–O bending vibrations in SnO_2, respectively.[7] The bands located at ~1678, 3054 and 3505 cm^{-1} are ascribed to O–H group owing from the water absorption or *via* chemical reactions (1)–(7) or may be from the surfactant doping.[7] FTIR spectrum of ZnO nanoparticles also comprised of dopant bands along with an intense characteristic broad band of ZnO at ~490 cm^{-1}. However, this broad band generally composed of two bands located at ~437 and 505 cm^{-1}, which are attributed to E_2 mode of hexagonal ZnO, which is a Raman active mode and oxygen deficiency/vacancy (VO) defect in ZnO, respectively.[24,34]

The bands observed at ~1384 and 1616 cm^{-1} are associated with the symmetric and asymmetric stretching in carboxylate, respectively.[34,35] The doublet located between 2800 to 3000 cm^{-1} is attributed to C–H stretching vibration in alkane group, whereas, the broad band located at ~3450 cm^{-1} is ascribed to O–H stretching mode of hydroxyl group.[26] All these bands are present in both types of metal oxides. The other bands located between 1000 to 4000 cm^{-1} in FTIR spectra of ZnO and SnO_2 are related to the carboxylate and hydroxyl impurities comes from environmental exposure due to hygroscopic nature of metal oxides.[26]

Raman spectrum of SnO_2 nanoparticles (Fig. 4(b)) has several Raman and IR active bands. The bands located at 476, 633 and 777 cm^{-1} are assigned to first-order Raman active modes, E_g, A_{1g} and B_{2g} of rutile phase of SnO_2. In these Raman active modes only the oxygen atoms vibrate, whereas, Sn atoms remains in stationary state. The modes B_{2g} and A_{1g} oscillate in the plane perpendicular to the *c*-axis, whereas, the E_g mode vibrates in the direction parallel to the *c*-axis.[12,24,25,36,37] The band located at 587 cm^{-1} is associated with the amorphous SnO_2 hydrous oxide.[12,24,37] But, the XRD pattern of tin oxide has well defined peaks that confirm the crystalline nature of the nanoparticles, which also observed from the HRTEM studies. Thus, this cannot be assigned to amorphous phase and may be arises due to reduced particle size, and defects related to surface as well as interface between the particles.[22,37] Dieguez *et al.*[37] demonstrated the effect of size of SnO_2 nanoparticles on the intensity of various Raman bands. The Raman spectrum of SnO_2 nanoparticles of size about 15 nm is well matched with Raman spectrum of same size of SnO_2 nanoparticles reported by Dieguez *et al.*[37] Besides these SnO_2 characteristic modes of vibration, some more bands are also observed at 144, 249 and 305 cm^{-1} in the Raman spectrum of SnO_2. However, these bands are not generally observed in the Raman spectrum of SnO_2, may arise due to surface defects. The bands at 249 and 305 can be assigned to E_u (LO) Raman mode and hydrolysis of $SnCl_4$, respectively.[25]

On the other hand, Raman spectrum of ZnO (Fig. 3(b)) composed of several characteristic optical bands of ZnO located at ~98, 330, 383, 438, 521 and 580 cm^{-1} that are attributed to the E_2 (low), E_2 (high)–E_2 (low), A_1 (TO), E_2 (high), E_1 (TO), and E_1 (LO) modes, respectively.[10,12,13,31] The presence of highly intense band around 438 cm^{-1} associated with non-polar optical phonon E_2 (high) mode of ZnO articulated by oxygen atoms, suggest the formation of high quality ZnO crystal.[12,13] The E_2 (low) and E_2 (high) modes are associated to the vibration of the heavy Zn sublattice or defects induced during synthesis and the mode involves only the oxygen atoms, respectively. The Raman active mode at ~438 cm^{-1} is ascribed to the E_2 mode for wurtzite ZnO crystals with very sharp features and this mode is also IR active as observed from FTIR studies. Apart from these bands, some other bands also present in the Raman spectrum of ZnO at ~980 and 1050 cm^{-1}, which are related with the carbon content (carboxylate, *etc.*) doped in ZnO.

Gas sensing behavior of metal oxide nanoparticles

The gas sensing behavior of the prepared metal oxide (SnO_2 and ZnO) nanoparticles have been recorded in ammonia environment at 46 ppm at different temperatures in the range of 60–200 °C. It has been observed that the electrical resistance of both the samples (SnO_2 and ZnO) decreases in ammonia environment (Fig. 5(a)). However, with the removal of ammonia from the testing chamber, the nanoparticles regain their original state. The observed behavior of the nanoparticles is well matched with reported behavior of metal oxide nanoparticles in ammonia environment.[10–12] The change in electrical resistance of the metal oxide samples with change of environment is converted into sensing response by using the relation,[7]

$$\text{Response } (\%) = \frac{R_a - R_g}{R_a} \times 100 \quad (8)$$

where, R_a and R_g are the resistances of the sample in air and ammonia environments, respectively. Fig. 5(a) and (b) show the gas sensing behavior of the SnO_2 and ZnO nanoparticles at 46 ppm ammonia at 100 °C, respectively. It is observed that as soon as the samples are exposed to ammonia gas, the electrical resistance of the samples sharply decrease and sensing

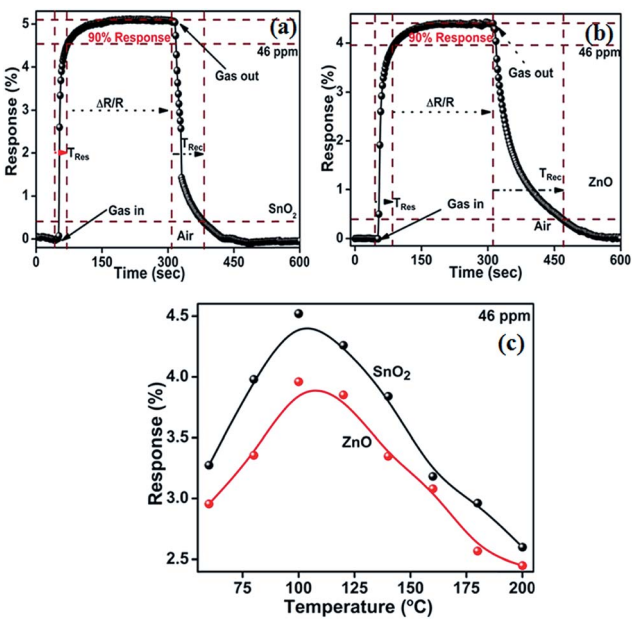

Fig. 5 Gas sensing behavior of (a) SnO_2, (b) ZnO nanoparticles in ammonia environment at 100 ppm as a function of time (c) as a function of temperature.

response rapidly increases and finally the sensing responses get saturated. As soon as the gas is removed from the cell, again the resistances of the samples increase and sensing responses decrease. The ammonia gas sensing response of the prepared metal oxide (SnO_2 and ZnO) nanoparticles has also been measured at different temperature (Fig. 5(c)). It has been observed that the sensing responses of both the samples increase up to 100 °C and again decreases with rise in temperature. The temperature dependent sensitivity of the metal oxide nanoparticles can be divided into three temperature regions. At low temperature, the oxygen molecules (O_2) are generally physisorbed on the metal oxide surface and captured the electron from the interior of the metal oxide (O_2 (g) + e^- → O_2^- (ads)). This increase in the thickness of the depletion layer affects the sensing response of the metal oxide nanoparticles as

$$\text{Response} = \left(\frac{\Delta n}{n}\right) L_D \tag{9}$$

where, n is the charge carriers concentration, Δn is the change in carrier concentration in ammonia environment and L_D is the depletion length. The length of depletion layer strongly depend on the temperature as

$$L_D = \left(\frac{\varepsilon_0 kT}{ne^2}\right)^{1/2} \tag{10}$$

here, ε_0 is the static dielectric constant, k is the Boltzmann constant, T is temperature and e is the electronic charge. Thus, the thickness of the depletion layer increases with increase of temperature and hence, the sensing response. At the moderate temperature, the physisorbed oxygen species (O_2^-) converted into chemisorbed oxygen ($2O^-$) on the metal oxide surface (O_2^- (ads) + e^- → $2O^-$ (ads)) and the thickness of the depletion layer is maximum and hence, maximum sensing response at that temperature. At higher temperatures beyond the critical temperature, metal oxide sample shows typical semiconducting behavior, which results in decrease in the thickness of depletion layer and hence, the decrease in sensing response. In the present study, the critical operating temperature is found to be ~100 °C. Furthermore, it has been observed that the gas sensing response of the SnO_2 nanoparticles (4.52% at 100 °C) is greater than that of ZnO nanoparticles (3.96% at 100 °C). Rout *et al.*[12] reported about ~18% and 20% sensing response of the ZnO nanorods and SnO_2 nanoparticles at relatively higher ppm level (~800 ppm) at 100 °C. The higher sensing response of SnO_2 (1.72) as compared to ZnO (1.10) has also been reported in literature.[38] Khun *et al.*[11] were reported a quite higher sensing response of the SnO_2 nanoparticles at 50 ppm of ammonia, whereas, the sensing response of the SnO_2 nanoparticles (~4.52% at 100 °C) in the present study is comparable to the sensing response of SnO_2 nanorods (~6% at 300 °C) observed at relatively higher ppm level (100 ppm).[26] Bagal *et al.*[7] have also been observed somewhat higher sensitivity (10%) of the SnO_2 nanoparticle at 100 ppm of ammonia at 250 °C. Zeng *et al.*[39] observed a sensing response of ~5.8 at 350 °C for pure ZnO nanostructure, which is found to increase up to 8 times with Pd doping. Thus, the prepared nanoparticles have shown comparable gas sensing response at relatively lower temperature. The higher sensing response of SnO_2 nanoparticles than that of ZnO nanoparticles may be due to large surface area which provides larger number of active sites for interaction or surface activeness. The sensing responses of the samples are reported at the 90% of maximum resistance (response) as the response time is generally defined by the time taken by the sensor to acquire 90% of the maximum resistance in presence of target gas. The response (T_{res}) and recovery (T_{rec}) times of both the samples have also been measured at 90% of maximum response and 10% of maximum response (fall of 90% of response) after inserting the air in chamber, respectively. The response and recovery times for SnO_2 nanoparticles are 31 s and 66 s, whereas, for ZnO nanoparticles these times are 38 s and 156 s, respectively. This indicates that the response and recovery time is lower for the SnO_2 nanoparticles as compared to ZnO nanoparticles at the same temperature (100 °C) and same ppm level of ammonia (46 ppm). The gas sensing behavior of the prepared nanoparticles at a fixed temperature can be understood by several mechanisms of interaction of nanostructured metals oxide with environment (Fig. 5). The metal oxide grains and their grain boundaries are always covered with adsorbed oxygen molecules. These adsorbed oxygen molecules pull out the electrons from the conduction band of the metal oxide due to large electronegativity of oxygen molecules, which results in the formation of oxygen ions (O_2^-, O^- and O^{2-}) adsorbed at the surface of metal oxide (Fig. 6(a)).[5–8,10–13] These processes can be understood by the chemical reactions as follows

$$O_2\ (g) + e^- \rightarrow O_2^-\ (ads) \tag{11}$$

$$O_2\ (g) + e^- \rightarrow 2O^-\ (ads) \tag{12}$$

$$O^-\ (ads) + e^- \rightarrow O^{2-}\ (ads) \tag{13}$$

In these electrons trapping processes, the free charge carrier concentration decreases due to removal of electrons from the metal oxide surface and the formation of a depletion layer (L_D) takes place at grain boundaries (Fig. 6(d)). The smaller sized nanoparticles have apparently larger number of active sites obtained from the enhanced oxygen vacancy defects present at the surface of nanoparticles. This results in more adsorption of oxygen molecules on the surface of nanoparticles which causes the upward band bending at the grain boundaries. This upward band bending restricted the motion of charge carriers. The surface depletions marginally affect the mobility and density of electron but have a great effect on the potential barrier height between nanoparticles. The generation of depletion region on the surface *via* electron trapping, narrow down the conducting path of electrons and increase potential barrier between the nanoparticles. This strongly influenced the electrical properties of metal oxide sample and the effect of the thickness of depletion layer on the potential barrier ($\varnothing_B$) can be given by the relation

$$\varnothing_B = \left(\frac{N_d e^2}{2\varepsilon_0}\right) {W_D}^2 \tag{14}$$

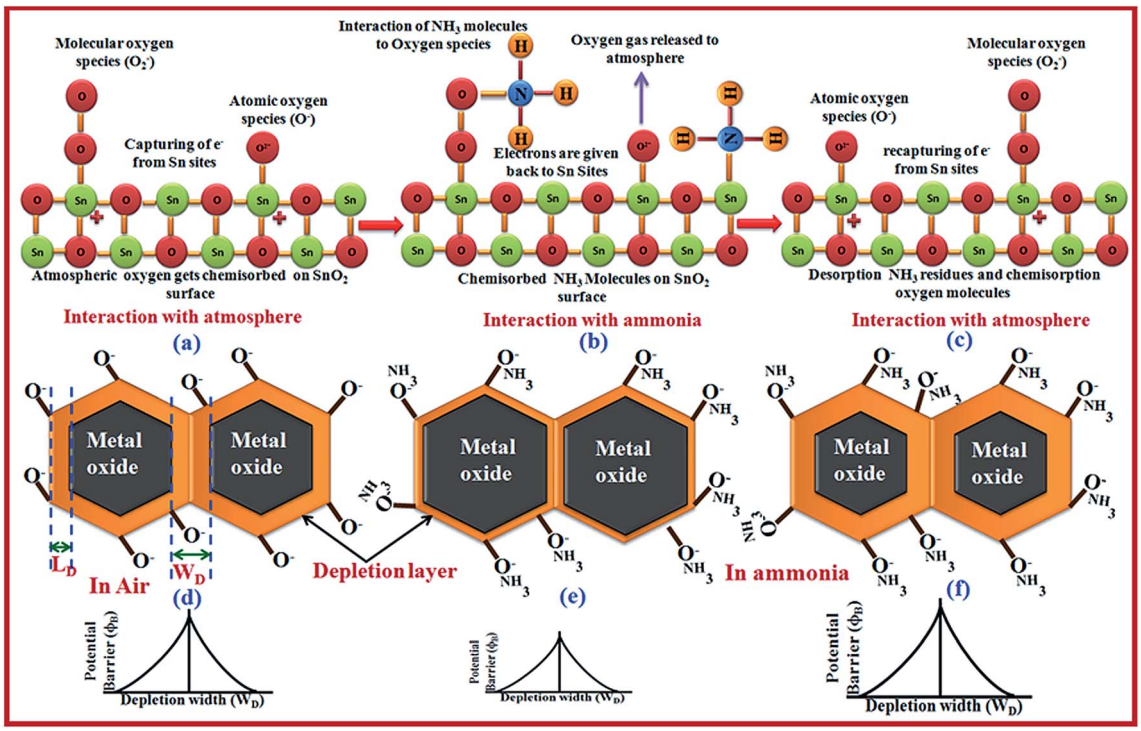

Fig. 6 Schematic of interaction of ammonia gas with metal oxide nanoparticles.

where, N_d is donor density and W_D depletion width. This will result in an increase in electrical resistance of metal oxide nanoparticles. Contrary to this, on exposing the oxide nanoparticles with reducing gas like NH_3, the oxygen species interact with NH_3 molecules to release the electrons to the conduction band (Fig. 6(b)). Such mechanism of gas sensing in ammonia environment can be given by the chemical reaction[11,12]

$$2NH_3 + 3O^- \text{ (ads)} \rightarrow N_2 + 3H_2O + 3e^- \quad (15)$$

These free electrons are again given back to the conduction band of metals oxide that results in decrease in depletion length (Fig. 6(e) in ammonia), which results in a decrease potential barrier height between nanoparticles and increase in carrier concentration to great extend. This will cause in a decrease of electrical resistance of the metal oxides in ammonia environment. The dependence of electrical resistance on the potential barrier height can be given by the relation[40]

$$R = R_0 \exp\left(\frac{-e\varnothing_B}{kT}\right) \quad (16)$$

Thus, the gas sensing response of the prepared samples partially derived by the change in electrical resistance by the modulation of the potential barrier of the junction of grains and represented by relation[40]

$$\text{Response} = \exp\left(\frac{-e\Delta\varnothing_B}{kT}\right) \quad (17)$$

However, in ammonia environment, there is one more possibility of formation of NO_x, in the presence of oxygen species as represented by the chemical reaction as[11]

$$4NH_3 + 5O_2^- \rightarrow 4NO + 6H_2O + 5e^- \quad (18)$$

In such formation of oxidizing NO_x, the thickness of depletion layer increases (Fig. 6(f) in ammonia) resulting in increase of electrical resistance of metal oxides. But the electrical resistance of our samples decreases in ammonia environment which rules out such gas sensing mechanism for the present samples. The nanostructured materials have larger aspect ratio for large adsorption–desorption of gas molecules, and thus, have higher sensing response.[6] On exposing again with atmosphere, the residues of NH_3 molecules are desorbed and oxygen species get chemisorbed on the surface of the metal oxide (Fig. 6(c)) and hence, the electric resistance of the sample increases.

For experimental realization of above discussed mechanism and to investigate the effect of ammonia gas on the molecular structure of metal oxide nanoparticles, FTIR spectra of ZnO and SnO_2 (Fig. 7(a) and (b)) were recorded in ammonia environment at different time of exposure at room temperature. Fig. 7(a) shows the FTIR spectra of SnO_2 nanoparticles recorded at 0–3 min ammonia exposure. The recovery of the samples has also been tested by recording the FTIR spectra after 3 min (3 min rec) of flush out of ammonia from measurement cell. Surprisingly, the intensity of the broad band located in the range of 400–750 cm^{-1} associated with the overlapped bands of Sn–O–Sn and O–Sn–O or asymmetric and symmetric stretching vibration bands of SnO_2 is found to decrease with ammonia

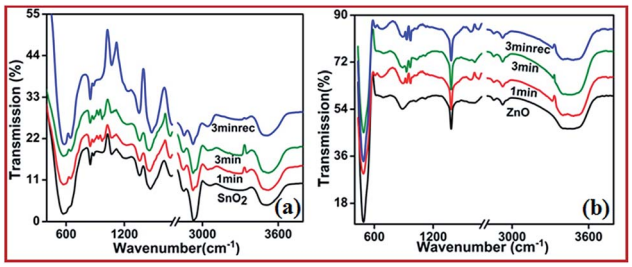

Fig. 7 FTIR spectra of (a) SnO_2 and (b) ZnO nanoparticles taken in ammonia environment at different exposure time.

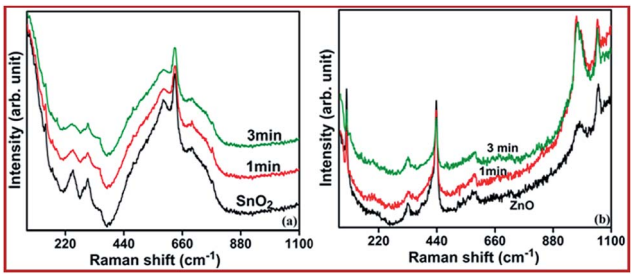

Fig. 8 Raman spectra of (a) SnO_2 and (b) ZnO nanoparticles taken in ammonia environment at different exposure time.

exposure time along with decrease in FWHM value of this band. The decrease in intensity of this band can be attributed to the removal of surface oxygen or deficiency of oxygen at –Sn– atom. The decrease in the FWHM value of this band can be attributed to the transition of O–Sn–O to Sn–O–Sn, with the removal of oxygen atom. The removed oxygen atom interacts with the ammonia molecule to form localized water molecule as per the chemical reaction (15). In this process of removal of oxygen from the surface or grain boundaries of the metal oxide nanoparticles cause a decrease in depletion length and hence, the electrical resistance.[5,7,8,10–13] However, the intensity of this band again increases with the removal of ammonia from the chamber and adsorption of new oxygen atoms at the grain boundaries. This results in an increase in depletion length and electrical resistance in air ambient, which suggest the recovery of the prepared nanoparticles.[10–13]

In addition to this, bands associated with the C–H stretching vibration of methyl and methylene present in the spectra of SnO_2 that might be due to doping of surfactant, also affected by the ammonia environment and the intensity of these bands decreases with ammonia exposure time, with minor shifting of the band located ~2926 cm^{-1}. The bands located ~1464 cm^{-1} also shift towards lower wavenumber side along with increase in intensity of this band (Fig. 7(a)). Similar to SnO_2, the molecular structure of ZnO also gets altered in ammonia environment. It is evident from the Fig. 7(b) that the intensity of the characteristic band of ZnO associated with the E_2 mode of ZnO and oxygen vacancy located at ~490 cm^{-1} decrease along with ammonia exposure time from 0 to 3 min and again recovered with removal of ammonia from the measurement cell within 3 min (3 min rec). The finger print region of FTIR spectrum of ZnO related to oxygen vacancy and carboxylate group, *etc.* also gets modified with ammonia exposure time (Fig. 6(b)). Moreover, it can be seen that the intensity of the O–H band (~3450 cm^{-1}) increases with ammonia exposure time (0–3 min), that may be due increase of O–H group *via* the chemical reaction (15) or (18) with the formation of localized water molecules at the surface of ZnO. Such type of effect also observed for SnO_2 nanoparticles (Fig. 7(a)). The other bands present in the FTIR spectra of ZnO also have similar behavior as that observed in case of SnO_2 nanoparticles in ammonia environment. The molecular structure of ZnO also recovered in air ambient. This suggests that the gas environment (ammonia) interact with the surface as well as interstitial oxygen of metal oxide that the change molecular structure of metal oxide nanoparticles and responsible for the change in optical and electrical properties with change of environment.

The effect of ammonia environment on the molecular structure of SnO_2 and ZnO has also been investigated under Raman spectroscopy technique (Fig. 8) at room temperature. It has been observed that the intensity of band located at ~249, 305 and 587 cm^{-1}, E_u (LO) Raman mode, hydrolysis of $SnCl_4$ and SnO_2 hydrous oxide, respectively, decreases significantly. However, the other bands are not significantly influenced by ammonia at room temperature. The Raman spectrum of ZnO nanoparticles also influences by ammonia. The intensity of the Raman bands of ZnO located at 98 and 438 cm^{-1}, related with the E_2 (low) and E_2 (high) decreases, whereas, the intensity of the band located at 980 cm^{-1} increases significantly with ammonia exposure time. The band located at 980 cm^{-1} also shifts towards the lower wavenumber (at 969 cm^{-1}) in ammonia environment. When metal oxide nanoparticles exposed to ammonia, the ammonia molecules dissociate and interact with the oxygen molecules in the lattice of SnO_2 or ZnO to form a localized water molecules. This causes a deficiency of oxygen ion leaving behind Sn or Zn ion, which results in a decrease in various Raman bands, whereas, the increase in intensity of Raman band at 980 cm^{-1} in ZnO could be due to attachment of locally generated OH^- ion with carbon content in ZnO structure or increase in the concentration of OH^- group on the surface of ZnO nanoparticles. These Raman spectroscopic results on SnO_2 and ZnO confirm the room temperature sensing ability of the prepared nanoparticles.

4. Conclusions

SnO_2 and ZnO nanoparticles were prepared by surfactant mediated facial hydrothermal process. The prepared SnO_2 nanoparticles have rutile phase, whereas, ZnO nanoparticles have wurtzite phase, depicted from XRD measurements. HRTEM study suggests the formation of hexagonal shaped nanoparticles for both SnO_2 and ZnO with particle size ~15 and 20 nm, respectively. The quite similar shaped of both type of oxides might be due to formation of similar type of surfactant cage for capping these metal oxide nanoparticles. FTIR and Raman studies also confirm the formation of both SnO_2 and ZnO nanoparticles with some doping of surfactant chains. The

gas sensing response of the prepared nanoparticle has been recorded in ammonia environment. The sensing responses of the SnO_2 and ZnO nanoparticles are found to be 4.53 and 3.96% at 46 ppm of ammonia at 100 °C. The electrical resistance of the prepared nanoparticles decreases due to decrease in width of depletion layer in ammonia environment. The FTIR and Raman spectroscopic measurements performed in ammonia environment, suggest the interaction of ammonia molecules with the oxygen molecules at the grain boundaries, which causes the formation of localized water molecules. This will tune the width of depletion layer and hence, responsible for gas sensing behavior of the nanoparticles.

Acknowledgements

Author is grateful to Dr Amarjeet Kaur, Department of Physics and Astrophysics, University of Delhi, Delhi for providing her lab facility for the synthesis and characterization. University Science Instrumentation Centre, University of Delhi, Delhi is gratefully acknowledged for providing characterization facilities.

References

1 S. Gubbala, V. Chakrapani, V. Kumar and M. K. Sunkara, *Adv. Funct. Mater.*, 2008, **18**, 2411.
2 Y. Yu, C. H. Chen and Y. Shi, *Adv. Mater.*, 2007, **19**, 993.
3 X. W. Lou, C. M. Li and L. A. Archer, *Adv. Mater.*, 2009, **21**, 2536.
4 T. Asari and T. Sato, *J. Phys. Soc. Jpn.*, 1997, **66**, 1360.
5 A. Afzal, N. Cioffi, L. Sabbatini and L. Torsi, *Sens. Actuators, B*, 2012, **171–172**, 25.
6 J. Riu, A. Maroto and F. X. Rius, *Talanta*, 2006, **69**, 288.
7 L. K. Bagal, J. Y. Patil, I. S. Mulla and S. S. Suryavanshi, *Ceram. Int.*, 2012, **38**, 4835.
8 B. Y. Wei, M. C. Hsu, P. G. Su, H. M. Lin, R. J. Wu and H. J. Lai, *Sens. Actuators, B*, 2004, **101**, 81.
9 L. N. Geng, S. R. Wang, P. Li, Y. Q. Zhao, S. M. Zhang and S. H. Wu, *Chin. J. Inorg. Chem.*, 2005, **21**, 977.
10 B. Renganathan, D. Sastikumar, G. Gobi, N. R. Yogamalar and A. C. Bose, *Opt. Laser Technol.*, 2011, **43**, 1398.
11 K. K. Khun, A. Mahajan and R. K. Bedi, *J. Appl. Phys.*, 2009, **106**, 124509.
12 C. S. Rout, M. Hegde, A. Govindaraj and C. N. R. Rao, *Nanotechnology*, 2007, **18**, 205504.
13 M. Zhao, X. Wang, J. Cheng, L. Zhang, J. Jia and X. Li, *Curr. Appl. Phys.*, 2013, **13**, 403.
14 G. Zhang and M. Liu, *Sens. Actuators, B*, 2000, **69**, 144.
15 T. Seiyama, A. Kato, K. I. Fujish and M. Nagatani, *Anal. Chem.*, 1962, **34**, 1502.
16 B. Shouli, C. Liangyuan, L. Dianqing, Y. Wensheng, Y. Pengcheng, L. Zhiyong, C. Aifan and C. C. Liu, *Sens. Actuators, B*, 2010, **146**, 129.
17 L. Jiang, G. Sun, Z. Zhou, S. Sun, Q. Wang, S. Yan, H. Li, J. Tian, J. Guo, B. Zhou and Q. Xin, *J. Phys. Chem. B*, 2005, **109**, 8774.
18 Y. Wu, N. Na, S. Zhang, X. Wang, D. Liu and X. Zhang, *Anal. Chem.*, 2009, **81**, 961.
19 S. Li, J. Zheng, W. Zhang, J. Cao, S. Li and Z. Rao, *Analyst*, 2013, **138**, 916.
20 N. Na, S. Zhang, S. Wang and X. Zhang, *J. Am. Chem. Soc.*, 2006, **128**, 14420.
21 J. Zheng, Z. Xue, S. Li, S. Li and Z. Rao, *Anal. Methods*, 2012, **4**, 2791.
22 J. Zheng, W. Zhang, J. Cao, X. Su, S. Li, S. Hu, S. Li and Z. Rao, *RSC Adv.*, 2014, **4**, 21644.
23 A. Joshi, S. A. Gangal and S. K. Gupta, *Sens. Actuators, B*, 2011, **156**, 938.
24 L. Z. Liu, T. H. Li, X. L. Wu, J. C. Shen and P. K. Chu, *J. Raman Spectrosc.*, 2012, **43**, 1423.
25 M. N. Rumyantseva, A. M. Gaskov, N. Rosman, T. Pagnier and J. R. Morante, *Chem. Mater.*, 2005, **17**, 893.
26 X. Zhou, W. Fu, H. Yang, Y. Zhang, M. Li and Y. Li, *Mater. Lett.*, 2013, **90**, 53.
27 F. Li, Y. Ding, P. Gao, X. Xin and Z. L. Wang, *Angew. Chem., Int. Ed. Engl.*, 2004, **43**, 5238.
28 I. Rawal and A. Kaur, *Sens. Actuators, A*, 2013, **203**, 92.
29 S. Pandey, G. K. Goswami and K. K. Nanda, *Sci. Rep.*, 2013, **3**, 2082.
30 S. Cho, S. Kim, E. Oh, S. H. Jung and K. H. Lee, *CrystEngComm*, 2009, **11**, 1650.
31 H. Niu, Q. Yang, F. Yu, K. Tang and Y. Xie, *Mater. Lett.*, 2007, **61**, 137–140.
32 L. Xu, Y. Guo, Q. Liao, J. Zhang and D. Xu, *J. Phys. Chem. B*, 2005, **109**, 13519.
33 P. Liu, Y. Li, Y. Guo and Z. Zhang, *Nanoscale Res. Lett.*, 2012, **7**, 220.
34 G. Xiong, U. Pal, J. G. Serrano, K. B. Ucer and R. T. Williams, *Phys. Status Solidi C*, 2006, **3**, 3577.
35 J. J. Max and C. Chapados, *J. Phys. Chem. A*, 2004, **108**, 3324.
36 P. G. Mendes, M. L. Moreira, S. M. Tebcherani, M. O. Orlandi, J. Andres, M. S. Li, N. Diaz-Mora, J. A. Varela and E. Longo, *J. Nanopart. Res.*, 2012, **14**, 750.
37 A. Dieguez, A. R. Rodrıguez, A. Vila and J. R. Morante, *J. Appl. Phys.*, 2001, **90**, 1550.
38 A. A. Tomchenko, G. P. Harmer, B. T. Marquis and J. W. Allen, *Sens. Actuators, B*, 2003, **93**, 126.
39 Y. Zeng, Z. Lou, L. Wang, B. Zou, T. Zhang, W. Zheng and G. Zou, *Sens. Actuators, B*, 2011, **156**, 395.
40 Y. Shi, M. Wang, C. Hong, Z. Yang, J. Deng, X. Song, L. Wang, J. Shao, H. Liu and Y. Ding, *Sens. Actuators, B*, 2013, **177**, 1027.

